
EFFICIENT-VDVAE: LESS IS MORE

Louay Hazami^{*†}
 Cash App Labs
 louay@squareup.com

Rayhane Mama^{*}
 Cash App Labs
 rayhane@squareup.com

Ragavan Thurairatnam
 Cash App Labs
 ragavan@squareup.com

ABSTRACT

Hierarchical VAEs have emerged in recent years as a reliable option for maximum likelihood estimation. However, instability issues and demanding computational requirements have hindered research progress in the area. We present simple modifications to the Very Deep VAE to make it converge up to $2.6 \times$ faster, save up to $20 \times$ in memory load and improve stability during training. Despite these changes, our models achieve comparable or better negative log-likelihood performance than current state-of-the-art models on all 7 commonly used image datasets we evaluated on. We also make an argument against using 5-bit benchmarks as a way to measure hierarchical VAE's performance due to undesirable biases caused by the 5-bit quantization. Additionally, we empirically demonstrate that roughly 3% of the hierarchical VAE's latent space dimensions is sufficient to encode most of the image information, without loss of performance, opening up the doors to efficiently leverage the hierarchical VAEs' latent space in downstream tasks. We release our source code and models at <https://github.com/Rayhane-mamah/Efficient-VDVAE>.

Keywords Unsupervised representation learning, Hierarchical VAE, Very deep VAE

1 Introduction

Maximum likelihood models have garnered a lot of attention from researchers in the last few years. Deep autoregressive models[1, 2, 3, 4] have long achieved the best log likelihoods across different modalities. Variational Autoencoder[5, 6] (VAE) is a different type of maximum likelihood models that are usually associated with representation learning [7, 8] and are known to generate subjectively more diverse images[9] compared to other generative approaches like diffusion models [10, 11, 12] and GANs [8, 13, 14, 15]. Very Deep VAE (VDVAE) [16], a newly proposed hierarchical VAE (HVAE), shows great promise in competing with deep autoregressive models in Maximum Likelihood Estimation (MLE). However, this method has proven to be computationally costly and to be generally unstable during training. In this paper, we aim to tackle these two issues and to share some of our insights that we have gathered throughout our experiments with VDVAE.

We start this work with a background on VAEs and HVAEs in section 2 and list similar works to VDVAE in section 3. Both these sections can be skipped by practitioners who are familiar with HVAEs.

In section 4, we introduce Efficient-VDVAE, which encompasses our contributions and tackles both the instability and compute cost problems associated with VDVAE.

We kick off the section 5 by empirically showing the impact of our approach. We then provide evaluations of our model trained on 7 commonly used benchmarks and show that our models are either on par with VDVAE or better in terms of Negative Log Likelihood (NLL) on all datasets. We also share some generated samples from the prior distribution of our model.

We then interpret the Efficient-VDVAE from an informational theory perspective in section 6, and we show the dilemma between that interpretation and the current dominant HVAE implementations, demonstrating along the way that commonly used 5-bit benchmarks are not suitable benchmarks for HVAEs.

^{*}Equal contribution.

[†]To whom correspondence should be addressed.

Finally, in section 7, we examine the size of the "effective latent space" of the Efficient-VDVAE and illustrate that one can prune 97% of the latent space without harming reconstruction quality, opening up the doors for a more effective usage of the HVAE's latent space in downstream tasks.

For practitioners interested in using VDVAE based models, we provide tips and insights gained from this work in the supplemental material C.

2 Background

2.1 Variational AutoEncoders

The goal of VAEs is to learn a generative model parametrized with θ of a joint distribution $p_\theta(x, z)$ that is usually factorized as:

$$p_\theta(x, z) = p_\theta(x|z)p_\theta(z) \quad (1)$$

where $p_\theta(z)$ is a prior distribution over latent variables z and $p_\theta(x|z)$ is the likelihood function (usually called stochastic decoder) that generates a data sample x from its latent variables z . VAEs are trained with the Evidence Lower Bound (ELBO):

$$\log p_\theta(x) \geq \mathbb{E}_{q_\phi(z|x)} [\log p_\theta(x|z)] - D_{\text{KL}} [q_\phi(z|x) || p_\theta(z)] \quad (2)$$

Where D_{KL} is the Kullback–Leibler divergence and $q_\phi(z|x)$ is the approximate posterior parametrized with ϕ . Usually in typical VAEs, $q_\phi(z|x)$ and $p_\theta(z)$ are modeled with Gaussian distributions. For a derivation of the ELBO and a more in depth introduction to VAEs, see [17].

2.2 Hierarchical Variational AutoEncoders

While fully factorized Gaussian $q_\phi(z|x)$ and $p_\theta(z)$ VAEs are theoretically capable of modeling any complex data distribution $p(x)$, in practice they are usually unable to learn such a solution due to computational constraints and a difficult optimization landscape[18]. To help alleviate this problem, deep HVAEs [19, 20, 21, 22] have been proposed in recent years as a way to increase the expressiveness of both the approximate posterior and the prior distributions, such as:

$$p_\theta(z) = p_\theta(z_1) \prod_{i=2}^L p_\theta(z_i|z_{<i}) \quad (3)$$

$$q_\phi(z|x) = q_\phi(z_1|x) \prod_{i=2}^L q_\phi(z_i|x, z_{<i})$$

$$p_\theta(x|z) = p_\theta(x|z_L)p_\theta(z) = p_\theta(x|z_L)p_\theta(z_1) \prod_{i=2}^L p_\theta(z_i|z_{<i}) \quad (4)$$

where L is the total number of latent hierarchical variables $z = \{z_1, z_2, \dots, z_L\}$. This formulation is known as the *top-down inference* (or *bidirectional inference*) HVAE introduced in [21]. Figure 4 gives a general overview of this process.

By substituting the hierarchical stochastic encoder, stochastic decoder and prior expressions in equation (2), we obtain the Hierarchical ELBO that HVAEs are trained to maximize:

$$\log p_\theta(x) \geq \mathbb{E}_{q_\phi(z|x)} [\log p_\theta(x|z)] - D_{\text{KL}} [q_\phi(z_1|x) || p_\theta(z_1)] - \sum_{i=2}^L \mathbb{E}_{q_\phi(z_{<i}|x)} D_{\text{KL}} [q_\phi(z_i|x, z_{<i}) || p_\theta(z_i|z_{<i})] \quad (5)$$

3 Related Work

While HVAEs have been used on multiple occasions in literature [19, 21, 22], they became especially prominent in recent works when these models became deep enough to compete with state-of-the-art autoregressive models.

The most widely used base very deep HVAE models are NVAE [23] and VDVAE [16]. During training, the former relies on heavy regularization in the hopes of stabilizing the unbounded KL terms of (5) and the latter -while achieving better NLL than NVAE- is less stable due to lack of regularization; both these models being more computationally expensive the deeper the model gets.

This work is based on VDVAE in the aim of reducing its computational requirements and adding more training stability. For completeness, we provide details of the architecture we use in all of our experiments in figure 5. It is advisable to refer to the source code for more details.

4 Revisiting VDVAE

4.1 Compute reduction

Architecture design: VDVAE’s work[16] empirically demonstrates that networks in general benefit from more layers at higher resolutions (measured in NLL), suggesting that it is important to have latent variables that learn local image details at high resolution layers. Our investigation shows that the benefit of adding layers to the high resolution layers is only noticeable when comparing NLL metrics and doesn’t perceptively affect the model’s reconstructed or generated images. The addition of high resolution layers also drastically increases the memory requirements of the networks. Moreover, the NLL gains from adding high resolutions layers follows the rule of diminishing returns. We show that it is possible to design memory efficient VDVAEs that don’t affect NLL results.

Optimization: We study the effect of changing the optimization scheme in order to converge faster (fewer updates and faster clock time). We also train all our models with reduced batch sizes in order to save computational costs. These changes introduce more training instabilities. Therefore, we developed new methods to stabilize the models.

4.2 Stabilization

Gradient smoothing: One common problem with training deep Gaussian HVAEs is the very large gradients resulting from the unbounded KL term[16, 23], more specifically the gradients resulting from the inverse of the posterior standard deviation $1/\sigma_{posterior}$. While NVAE attempts to solve this by using residual normal distributions and clipping the range of the $\log(\sigma)$ predicted by the model, VDVAE counters this by clipping/skipping sharp gradients. In practice, we find that these solutions can hinder the model’s learning depending on the dataset and depending on the model’s other hyper-parameters. We propose instead to smooth the gradients of the inverse std by computing the Gaussian stds of both posteriors and priors with $\sigma = \text{Softplus}(y, \beta) = \frac{1}{\beta} \log(1 + \exp(\beta y))$, with y the activation of a linear layer and β being a smoothing multiplier smaller than 1. Like VDVAE, we use the discretized mixture of logistics (MoL) as the output layer of the generative model. To mitigate its sharp gradients, we similarly use gradient smoothing.

Optimizer: Since the norm of gradients of the MoL layer can be much larger than 1, especially when using small batch sizes, optimizing this model with the Adam optimizer [24] can prove to be challenging since its second momentum $v_t = \beta_2 v_{t-1} + (1 - \beta_2) g_t^2$ grows large. As such, we propose to use its infinite norm alternative, Adamax, which does not suffer from the same problem.

5 Experiments

5.1 Model design, NLL and memory

We first tested to what extent increasing the depth of the model in the higher resolution layers is useful for the NLL metric, and how much memory can be saved by reducing this depth without hurting the model performance. In table 1a, we train multiple networks while fixing the number of low resolution layers and we experiment with only changing the number of medium and high resolution layers. We conclude that, after a certain depth, increasing the number of layers in high resolution latent spaces stops improving MLE performance. Distributing the number of layers across the lower resolution layers, not only saves memory, but also preserves performance.

We then tested the impact of using the same big number of filters across all layers of the model against adopting an incremental strategy of the width, as can be seen in table 1b. We show that high resolution latent spaces benefit less

Distribution of Layers					Memory (GB)	NLL (bits/dim)
32 × 32	16 × 16	8 × 8	4 × 4	1 × 1		
11	15	19	7	6	66	3.63
16	15	19	7	6	71	3.61
16	25	19	7	6	76	3.58
25	25	19	7	6	88	3.58
41	20	10	7	6	99	3.59

(a) Distribution of layer depths.

Distribution of Layers					Memory (GB)	NLL (bits/dim)
32 × 32	16 × 16	8 × 8	4 × 4	1 × 1		
256	256	256	256	256	64	3.61
32	32	64	128	256	12	3.63
64	64	128	256	512	34	3.61
512	512	512	512	512	99	3.59

(b) Distribution of layer widths.

Table 1: **NLL and memory load with different configurations of stochastic layers on ImageNet 32 × 32** (similar trends appear on the other benchmarks). **(a):** Networks with fixed low resolution, but with different number of middle and high resolution layers. The addition of extra layers in high resolution is a diminishing returns endeavor. **(b):** Networks with 84 stochastic layers, but with varying layer widths. Reducing the width of the model can save memory while getting comparable NLL results.

Batch size	Without gradient smoothing		With gradient smoothing	
	NLL (bits/dim)	Skipped updates	NLL (bits/dim)	Skipped updates
4	3.25	78	3.22	5
8	3.11	8	3.11	4
32	2.97	3	2.97	0

(a) Gradient smoothing and batch size.

Dataset	Without gradient smoothing	With gradient smoothing
FFHQ 1024 × 1024	diverged	6
CelebAHQ 1024 × 1024	diverged	23

(b) High resolution datasets.

Table 2: **Effects of gradient smoothing.** (a) We trained networks with the same model architecture with varying the batch size for 500k steps and tested the effect of gradient smoothing at $\beta = \log(2)$. The gradient smoothing does not affect NLL and results in greater stability when the batch size is reduced, as measured by the number of skipped updates at a gradient update threshold of 800 (for a negative ELBO measured in nats/dim). These results are computed on the CIFAR-10 dataset, but other datasets exhibit similar behaviors. (b) Number of skipped updates in 80k steps on high resolution datasets for a threshold of 1200 (loss computed in nats/dim), $\beta = 0.4$ and a batch size of 8 . Gradient smoothing allows us to train models with small batch sizes.

from width than the lower resolution latent spaces. We take advantage of this finding to considerably reduce the GPU memory load while remaining comparable to the baseline. In all of our experiments, we set a maximum GPU memory load of 320GB.

5.2 Gradient smoothing and stability

Reducing the computation requirements by reducing the batch size as described in section 4.1 introduces training instabilities. We show in table 2 that gradient smoothing substantially improves stability when using small batch sizes and that it is mandatory for high resolution datasets. For completeness, we show the effect of gradient smoothing as a function of model depth in Appendix B.2.

5.3 Quantitative model results

5.3.1 Computation load comparison

We start by examining the training memory load gain between our Efficient-VDVAE and the original VDVAE. All VDVAE parameters are reported in the original VDVAE work³, and we train our models with only applying the architecture and optimization modifications described in section 4 and tested in experiments 5.1, 5.2.

In table 3, we report the results on CIFAR-10 [25], ImageNet 32 × 32, ImageNet 64 × 64 [26] and FFHQ 256 × 256 [27] datasets. In the worst case, Efficient-VDVAE has a $1.68 \times$ lower training memory load, converges in $1.38 \times$ less updates and trains $1.45 \times$ faster in clock time, while being consistently similar or better than the original VDVAE in terms of NLL. More compact Efficient-VDVAE configurations can also be trained to consume $20 \times$ less memory load, to converge in $2 \times$ less updates and to train in $2.6 \times$ less clock time on Imagenet 32 × 32. In this scenario, computational gains can worsen the NLL metric by up to 0.02% which is usually qualitatively indistinguishable.

³On occasions, the official released codebase parameters differs from what's reported in the paper. In that case we rely on the codebase version.

Dataset	CIFAR-10			Imagenet 32 × 32			Imagenet 64 × 64			FFHQ 256 × 256 (5-bits)		
	Model	C1	C2	VDVAE	C1	C2	VDVAE	C1	C2	VDVAE	C1	C2
Layers	47	47	43	73	73	78	84	84	75	66	66	66
width	incr.	384	384	incr.	512	512	incr.	512	512	incr.	512	512
Batch size	16	16	32	64	64	256	32	32	128	16	16	32
Learning rate	0.001 ↘	0.001 ↘	0.0001	0.001 ↘	0.001 ↘	0.0001	0.001 ↘	0.001 ↘	0.0001	0.001 ↘	0.001 ↘	0.0001
Optimizer	Adamax	Adamax	Adam	Adamax	Adamax	Adam	Adamax	Adamax	Adam	Adamax	Adamax	Adam
Parameters	18M	51M	39M	52M	156M	119M	57M	168M	125M	66M	198M	115M
Time (h)	99	108	144	161	177	420	184	202	420	226	245	420
Training iter.	800k	800k	1.1M	800k	800k	1.7M	800k	800k	1.6M	850k	850k	1.7M
Memory (GB)	8	17	32	26	76	512	29	116	512	101	304	512
NLL (bits/dim)	≤ 2.91	≤ 2.87	≤ 2.87	≤ 3.60	≤ 3.58	≤ 3.80	≤ 3.33	≤ 3.30	≤ 3.52	≤ 0.61	≤ 0.60	≤ 0.61

Table 3: Computational load comparison. We train 2 configurations of Efficient-VDVAE, derived from the VDVAE baseline by only modifying the hyper-parameters described in section 4. We report the convergence speed as measured in number of iterations and clock time (in hours). We also report the total training memory load of each model and their NLL at convergence time. The configuration C1 is only different from C2 in the use of incremental filter width (experiment of table 1b). A south-east arrow (\searrow) denotes the use of cosine decay. More detailed model hyper-parameters are available in table 6 and the source code.

Model	MNIST	CIFAR-10	Imagenet 32 × 32	Imagenet 64 × 64	CelebA 64 × 64	CelebAHQ 256 × 256		FFHQ 256 × 256		CelebAHQ 1024 × 1024	FFHQ 1024 × 1024
						5-bits	8-bits	5-bits	8-bits		
ANF[32]	-	3.05	3.92	-	-	0.72	-	-	-	-	-
Flow++[33]	-	3.08	3.86	3.69	-	-	-	-	-	-	-
GLOW[34]	-	3.35	4.09	3.81	-	1.03	-	-	-	-	-
DenseFlow[35]	-	2.98	3.63	3.35	1.99	-	-	-	-	-	-
δ -VAE[36]	-	2.83	3.77	-	-	-	-	-	-	-	-
SPN[37]	-	-	3.85	3.52	-	0.61	-	-	-	-	-
MaCow[38]	-	3.16	-	3.69	-	0.67	-	-	-	-	-
PixelVAE++[3]	78.00	2.90	-	-	-	-	-	-	-	-	-
Locally Masked PixelCNN[39]	77.58	2.89	-	-	-	0.74	-	-	-	-	-
Image Transformer[40]	-	2.89	3.77	-	-	-	-	-	-	-	-
Sparse Transformer[41]	-	2.80	-	3.44	-	-	-	-	-	-	-
Aug. Sparse Transformer[4]	-	2.53*	-	-	-	-	-	-	-	-	-
UDM[42]	-	3.04	-	-	1.93	-	-	-	-	-	-
VDM[43]	-	$\leq 2.49^*$	$\leq 3.72^*$	$\leq 3.40^*$	-	-	-	-	-	-	-
NVAE[23]	≤ 78.01	≤ 2.91	≤ 3.92	-	≤ 2.03	≤ 0.70	-	≤ 0.69	-	-	-
VDVAE[16]	-	-	≤ 2.87	≤ 3.80	≤ 3.52	-	-	-	≤ 0.61	-	≤ 2.42
CR-NVAE[44]	$\leq 76.93^*$	$\leq 2.51^*$	-	-	$\leq 1.86^*$	-	-	-	-	-	-
Efficient-VDVAE	-	-	≤ 2.87	≤ 3.58	≤ 3.30	≤ 1.83	≤ 0.57	-	≤ 0.60	-	-
Efficient-VDVAE (section 6)	≤ 79.09	≤ 2.87	≤ 3.58	≤ 3.30	≤ 1.83	≤ 0.51	≤ 1.35	≤ 0.53	≤ 2.17	≤ 1.01	≤ 2.30

Table 4: Comparison against state-of-the-art likelihood-based generative models. Unless otherwise specified, all datasets have 8-bit images. All benchmarks are in bits/dim except for MNIST benchmarks which are reported in nats. An asterisk (*) denotes scores with data augmentation. Since most models overfit on CIFAR-10, data augmentation greatly improves performance. Our computational efficiency allows us to set HVAE baselines on high resolution datasets. Efficient-VDVAE outperforms current state-of-the-art models on most datasets.

5.3.2 NLL results

In table 4, we report the NLL scores compared to other notable MLE models. We report these results on more datasets than in the original VDVAE for completeness: We add NLL results on MNIST[28], CelebA 64 × 64[29, 30], CelebAHQ 256 × 256 and CelebAHQ 1024 × 1024[31]. Most of these additions are commonly used except CelebAHQ 1024 × 1024 which we added to act as a baseline for high resolution images for future work. We also provide the 8-bit scores on FFHQ 256 × 256 and CelebAHQ 256 × 256 which are usually trained in 5-bits (see section 6 for an in-depth explanation).

Despite being more efficient than VDVAE, Efficient-VDVAE consistently achieves either similar or better NLL scores on all baselines. It also achieves state-of-the-art performance on all datasets but CIFAR-10, although it remains comparable to non-augmented models. See codebase for a rundown of all hyper-parameters used for each dataset.



(a) Imagenet 32×32 ($t = 0.85$).

(b) Imagenet 64×64 ($t = 0.9$).

(c) CelebA 64×64 ($t = 0.8$).



(d) CelebAHQ 256×256 5-bits ($t = 0.85$).

(e) FFHQ 256×256 5-bits ($t = 0.8$).



(f) CelebAHQ 256×256 8-bits ($t = 0.85$).

(g) FFHQ 256×256 8-bits ($t = 0.8$).

Figure 1: **Samples generated from the prior of Efficient-VDVAE with temperature (t)** (best viewed zoomed in). Compared to 5-bit images, the full depth color images don't have banding effects. They also introduce small details missing in 5-bit images (moles, freckles, light reflections, etc.). More samples are available in appendix D.2.

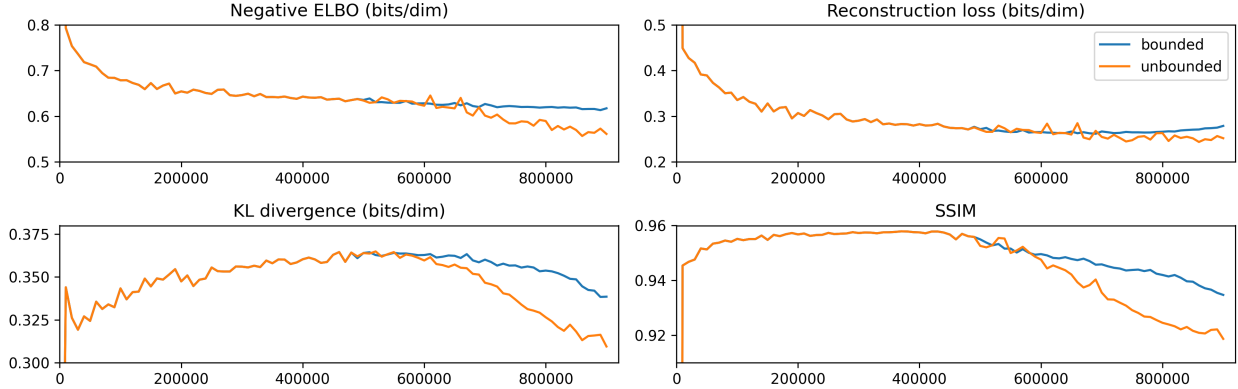


Figure 2: **Impact of the bound on metrics:** We compare the metrics of the bounded model and the unbounded model both trained on FFHQ 256×256 . We observe that the unbounded model has a lower reconstruction loss. We also observe that the KL divergence converges to a lower value which then allows the Negative ELBO to reach a better final value. This however does not reflect the overall closeness of the reconstructed images to the target images as demonstrated by the Structural Similarity Index Measure (SSIM)[46] values.

5.4 Qualitative model results

Figure 1 illustrates generated samples from the prior using the equation 4. We show a comparable subjective image quality and diversity to that of VDVAE. Although our models achieve a substantial improvement on the FFHQ 1024×1024 NLL compared to the VDVAE baseline, they are still not expressive enough to generate good high quality high resolution images. We show unconditional samples with different temperatures on FFHQ 1024×1024 and CelebAHQ 1024×1024 in D.2.

6 Information theoretic interpretation and output layer dilemma

6.1 Lossless compression

From an information theory perspective, the reconstruction loss is interpreted as the term that copies information from the pixel space to the latent space, and the KL divergence is interpreted as the regularization term that compresses that information[18, 45]. Thus, during training, we expect the reconstruction loss to decrease and the KL divergence to increase as more information gets stored in the latent space. When the reconstruction loss reaches a minimum at which it can no longer decrease, we expect the KL divergence term to decrease as information in the latent space gets compressed.

While empirically desirable, VAEs (and HVAEs) rarely achieve perfect reconstructions. This is in part due to a pre-existing limit on the sharpness of the output layer; the MoL layer in the case of VDVAE. While this has been originally implemented to preserve training stability[2], in our experiments it proved to be unnecessary after the gradient smoothing addition. We study the effect of removing such a bound in the next section.

6.2 Impact on 5-bit quantization

The removal of the bound on the MoL layer allows us to adhere more accurately to the principles of lossless compression, and more importantly, avoid training our networks in an over-regularized regime[18]. In table 4, we test the effect of this removal on FFHQ 256×256 and CelebAHQ 256×256 which have been consistently quantized to 5-bits in prior work [16, 23, 47, 48, 38, 37, 32, 39, 34]. We achieve much better NLL than state-of-the-art models on these 5-bit benchmarks. We report in figure 2 the evolution of the validation metrics of a bounded and an unbounded model on FFHQ 256×256 during training.

Qualitatively, the model appears to compress the latent space information attributed to the banding effect [49, 50] which is heavily present in the 5-bit target images. Figure 3 illustrates the appearance of banding effects in the 5-bit targets, and their effect on the unbounded models’ reconstructions. We show differences between unconditional generated samples in 8-bits and 5-bits in figure 1.



Figure 3: 5-bit quantization and banding effects on FFHQ 256×256 (best viewed zoomed in). From left to right: 5-bit targets, unbounded reconstruction, bounded reconstruction and finally the 8-bit targets. All on FFHQ 256×256.

% of used posteriors	Encoded dataset size (GB)	Negative ELBO	Reconstruction	KL divergence
2.5%	111	2.43	1.16	1.27
3%	133	2.20	1.05	1.15
4%	177	2.18	1.05	1.13
5%	222	2.17	1.04	1.13
7%	310	2.17	1.04	1.13
100%	4433	2.17	1.04	1.13

Table 5: Evolution of the encoded dataset (z) size and test costs (bits/dim) with the pruning of the latent posteriors on 8-bit FFHQ 256 × 256 (uncompressed pixels size is ≈ 50 GB). We observe that by only using 3% of the latent space, the encoded dataset size can be 33× smaller with a comparable negative ELBO results.

Although prior work[34] has introduced the use of the 5-bit benchmarks as a means to reduce the datasets' complexity by removing the high frequency color depth information, current state-of-the-art models are more capable of modeling the high frequency noise. Since VAEs are trained to mimic the training data distribution, and, any bias introduced in the data preparation makes them generate samples with a similar bias, they are expected to mimic the banding effect which is undesirable from a generative modeling perspective. Additionally, as HVAEs get more expressive, NLL differences on 5-bit datasets start to only contrast how well the models are compressing the banding effects, rather than giving a global sense of how well the HVAEs are learning the data distribution. Thus, we advocate that all future work should be evaluated on the 8-bit images. As a step in this direction, we provide in table 4 NLL scores for the 8-bit version of the FFHQ 256 × 256 and CelebAHQ 256 × 256 datasets.

Lastly, we observe in table 4, that the removal of the output bound does not affect the NLL results of the 8-bit benchmarks. We hypothesize that this is because our current models are not expressive enough to produce the same KL compression effect on full color depth images.

7 Effective latent space

In their dense form, z can occupy a lot of memory, especially with very deep HVAEs, which is not suitable for downstream tasks. Fortunately, in practice, VAEs (and HVAEs) train in a polarized regime and learn a latent space where the majority of the latent dimensions are "turned off" for all samples [51, 52].

We experiment with "pruning" the posteriors that are "turned-off" by replacing them with the prior and observe its effect on the test scores. By definition of the polarized regime[51], dimensions are turned-off when their average KL divergence (independent from the latent resolution) is lower than a certain threshold. We report, in table 5, the effect of moving the cutoff threshold on CelebAHQ 256 × 256 (these results hold for other datasets as well).

We discover that roughly 3% of the latent dimensions encode most of the information required to reconstruct the inputs as shown by an almost equal reconstruction loss. The remaining 97% posterior dimensions can be collapsed on the prior without any qualitative effects as seen in figure 6. Therefore, we theorize that using the "active dimensions" of the latent space alone could be sufficient for downstream tasks, while also being memory efficient.

8 Limitations and broader impact

This paper's contributions are based on the fundamental need for a cheaper and stabler version of the Deep HVAE. The contributions of this paper have been tested on commonly used datasets for a full comparison with current state-of-the-art. This work makes it more accessible to build applications in representation learning, content generation and semi-supervised learning.

Despite our work, HVAEs still require a relatively large amount of compute, especially on high resolution datasets, which can still make them inaccessible for individuals and small groups. From a stability point of view, very deep HVAEs that use unimodal latent distributions with infinite support remain, to some extent, unstable by design. Using different latent distributions [53, 54, 55, 56] may prove fruitful for completely stabilizing HVAEs. However, using different latent distributions while achieving the same NLL performance of the Gaussian distribution is still an open area of research.

9 Conclusion

In this paper, we show that VDVAE’s stability and computational efficiency could be improved while retaining or boosting the MLE performance as measured in NLL. We then argue against benchmarking on 5-bit quantized datasets, and we reason that future work should be evaluated on full color depth datasets. We also empirically show that only a minor percentage of HVAE’s sparse latent dimensions is responsible for encoding most of the information. In the spirit of making these models accessible, we have publicly released our source code.

Acknowledgments

The authors would like to thank Alex Krizhevsky for his mentorship and insightful discussions. The authors also thank Joe Palermo, Marc Tyndel, Hashiam Kadhim and Stephen Piron for their feedback and support.

References

- [1] Aaron Van den Oord, Nal Kalchbrenner, Lasse Espeholt, Oriol Vinyals, Alex Graves, et al. Conditional image generation with pixelcnn decoders. *Advances in neural information processing systems*, 29, 2016.
- [2] Tim Salimans, Andrej Karpathy, Xi Chen, and Diederik P Kingma. Pixelcnn++: Improving the pixelcnn with discretized logistic mixture likelihood and other modifications. *arXiv preprint arXiv:1701.05517*, 2017.
- [3] Hossein Sadeghi, Evgeny Andriyash, Walter Vinci, Lorenzo Buffoni, and Mohammad H Amin. Pixelvae++: Improved pixelvae with discrete prior. *arXiv preprint arXiv:1908.09948*, 2019.
- [4] Heewoo Jun, Rewon Child, Mark Chen, John Schulman, Aditya Ramesh, Alec Radford, and Ilya Sutskever. Distribution augmentation for generative modeling. In Hal Daumé III and Aarti Singh, editors, *Proceedings of the 37th International Conference on Machine Learning*, volume 119 of *Proceedings of Machine Learning Research*, pages 5006–5019. PMLR, 13–18 Jul 2020.
- [5] Diederik P Kingma and Max Welling. Auto-encoding variational bayes, 2014.
- [6] Danilo Jimenez Rezende, Shakir Mohamed, and Daan Wierstra. Stochastic backpropagation and approximate inference in deep generative models, 2014.
- [7] Yoshua Bengio, Aaron C. Courville, and Pascal Vincent. Unsupervised feature learning and deep learning: A review and new perspectives. *CoRR*, abs/1206.5538, 2012.
- [8] Alec Radford, Luke Metz, and Soumith Chintala. Unsupervised representation learning with deep convolutional generative adversarial networks. *arXiv preprint arXiv:1511.06434*, 2015.
- [9] Sam Bond-Taylor, Adam Leach, Yang Long, and Chris G. Willcocks. Deep generative modelling: A comparative review of vaes, gans, normalizing flows, energy-based and autoregressive models. *CoRR*, abs/2103.04922, 2021.
- [10] Jonathan Ho, Ajay Jain, and Pieter Abbeel. Denoising diffusion probabilistic models. *Advances in Neural Information Processing Systems*, 33:6840–6851, 2020.
- [11] Jascha Sohl-Dickstein, Eric Weiss, Niru Maheswaranathan, and Surya Ganguli. Deep unsupervised learning using nonequilibrium thermodynamics. In *International Conference on Machine Learning*, pages 2256–2265. PMLR, 2015.
- [12] Alexander Quinn Nichol and Prafulla Dhariwal. Improved denoising diffusion probabilistic models. In *International Conference on Machine Learning*, pages 8162–8171. PMLR, 2021.
- [13] Ian Goodfellow, Jean Pouget-Abadie, Mehdi Mirza, Bing Xu, David Warde-Farley, Sherjil Ozair, Aaron Courville, and Yoshua Bengio. Generative adversarial nets. *Advances in neural information processing systems*, 27, 2014.
- [14] Phillip Isola, Jun-Yan Zhu, Tinghui Zhou, and Alexei A. Efros. Image-to-image translation with conditional adversarial networks. *CoRR*, abs/1611.07004, 2016.
- [15] Jun-Yan Zhu, Taesung Park, Phillip Isola, and Alexei A. Efros. Unpaired image-to-image translation using cycle-consistent adversarial networks. *CoRR*, abs/1703.10593, 2017.
- [16] Rewon Child. Very deep {vae}s generalize autoregressive models and can outperform them on images. In *International Conference on Learning Representations*, 2021.
- [17] Diederik P. Kingma and Max Welling. An introduction to variational autoencoders. *CoRR*, abs/1906.02691, 2019.
- [18] Ronald Yu. A tutorial on vaes: From bayes’ rule to lossless compression. *CoRR*, abs/2006.10273, 2020.

- [19] Rajesh Ranganath, Dustin Tran, and David Blei. Hierarchical variational models. In *International conference on machine learning*, pages 324–333. PMLR, 2016.
- [20] Durk P Kingma, Tim Salimans, Rafal Jozefowicz, Xi Chen, Ilya Sutskever, and Max Welling. Improved variational inference with inverse autoregressive flow. In D. Lee, M. Sugiyama, U. Luxburg, I. Guyon, and R. Garnett, editors, *Advances in Neural Information Processing Systems*, volume 29. Curran Associates, Inc., 2016.
- [21] Casper Kaae Sønderby, Tapani Raiko, Lars Maaløe, Søren Kaae Sønderby, and Ole Winther. Ladder variational autoencoders. *Advances in neural information processing systems*, 29, 2016.
- [22] Alexej Klushyn, Nutan Chen, Richard Kurle, Botond Cseke, and Patrick van der Smagt. Learning hierarchical priors in vaes. *Advances in neural information processing systems*, 32, 2019.
- [23] Arash Vahdat and Jan Kautz. Nvae: A deep hierarchical variational autoencoder. *Advances in Neural Information Processing Systems*, 33:19667–19679, 2020.
- [24] Diederik P. Kingma and Jimmy Ba. Adam: A method for stochastic optimization, 2017.
- [25] Alex Krizhevsky, Vinod Nair, and Geoffrey Hinton. Cifar-10 (canadian institute for advanced research).
- [26] Jia Deng, Wei Dong, Richard Socher, Li-Jia Li, Kai Li, and Li Fei-Fei. Imagenet: A large-scale hierarchical image database. In *2009 IEEE conference on computer vision and pattern recognition*, pages 248–255. Ieee, 2009.
- [27] Tero Karras, Samuli Laine, and Timo Aila. Flickr faces hq (ffhq) 70k from stylegan. *CoRR*, 2018.
- [28] Yann LeCun and Corinna Cortes. MNIST handwritten digit database. 2010.
- [29] Ziwei Liu, Ping Luo, Xiaogang Wang, and Xiaou Tang. Deep learning face attributes in the wild. In *Proceedings of the IEEE international conference on computer vision*, pages 3730–3738, 2015.
- [30] Anders Boesen Lindbo Larsen, Søren Kaae Sønderby, Hugo Larochelle, and Ole Winther. Autoencoding beyond pixels using a learned similarity metric. In Maria Florina Balcan and Kilian Q. Weinberger, editors, *Proceedings of The 33rd International Conference on Machine Learning*, volume 48 of *Proceedings of Machine Learning Research*, pages 1558–1566, New York, New York, USA, 20–22 Jun 2016. PMLR.
- [31] Tero Karras, Timo Aila, Samuli Laine, and Jaakko Lehtinen. Progressive growing of gans for improved quality, stability, and variation. *CoRR*, abs/1710.10196, 2017.
- [32] Chin-Wei Huang, Laurent Dinh, and Aaron Courville. Augmented normalizing flows: Bridging the gap between generative flows and latent variable models. *arXiv preprint arXiv:2002.07101*, 2020.
- [33] Jonathan Ho, Xi Chen, Aravind Srinivas, Yan Duan, and Pieter Abbeel. Flow++: Improving flow-based generative models with variational dequantization and architecture design. In *International Conference on Machine Learning*, pages 2722–2730. PMLR, 2019.
- [34] Durk P Kingma and Prafulla Dhariwal. Glow: Generative flow with invertible 1x1 convolutions. *Advances in neural information processing systems*, 31, 2018.
- [35] Matej Grcić, Ivan Grubišić, and Siniša Šegvić. Densely connected normalizing flows. *Advances in Neural Information Processing Systems*, 34, 2021.
- [36] Ali Razavi, Aäron van den Oord, Ben Poole, and Oriol Vinyals. Preventing posterior collapse with delta-vaes. *CoRR*, abs/1901.03416, 2019.
- [37] Jacob Menick and Nal Kalchbrenner. Generating high fidelity images with subscale pixel networks and multidimensional upscaling. *arXiv preprint arXiv:1812.01608*, 2018.
- [38] Xuezhe Ma, Xiang Kong, Shanghang Zhang, and Eduard Hovy. Macow: Masked convolutional generative flow. *Advances in Neural Information Processing Systems*, 32, 2019.
- [39] Ajay Jain, Pieter Abbeel, and Deepak Pathak. Locally masked convolution for autoregressive models. In *Conference on Uncertainty in Artificial Intelligence*, pages 1358–1367. PMLR, 2020.
- [40] Niki Parmar, Ashish Vaswani, Jakob Uszkoreit, Lukasz Kaiser, Noam Shazeer, Alexander Ku, and Dustin Tran. Image transformer. In *International Conference on Machine Learning*, pages 4055–4064. PMLR, 2018.
- [41] Rewon Child, Scott Gray, Alec Radford, and Ilya Sutskever. Generating long sequences with sparse transformers. *arXiv preprint arXiv:1904.10509*, 2019.
- [42] Dongjun Kim, Seungjae Shin, Kyungwoo Song, Wanmo Kang, and Il-Chul Moon. Score matching model for unbounded data score. *CoRR*, abs/2106.05527, 2021.
- [43] Diederik P Kingma, Tim Salimans, Ben Poole, and Jonathan Ho. Variational diffusion models. *arXiv preprint arXiv:2107.00630*, 2021.

- [44] Samarth Sinha and Adji Bousso Dieng. Consistency regularization for variational auto-encoders. In A. Beygelzimer, Y. Dauphin, P. Liang, and J. Wortman Vaughan, editors, *Advances in Neural Information Processing Systems*, 2021.
- [45] Xi Chen, Diederik P Kingma, Tim Salimans, Yan Duan, Prafulla Dhariwal, John Schulman, Ilya Sutskever, and Pieter Abbeel. Variational lossy autoencoder. *arXiv preprint arXiv:1611.02731*, 2016.
- [46] Zhou Wang, A. Bovik, H. R. Sheikh, and E. P. Simoncelli. Image quality assessment: from error visibility to structural similarity. *IEEE Transactions on Image Processing*, 13:600–612, 2004.
- [47] Chris Finlay, Jörn-Henrik Jacobsen, Levon Nurbekyan, and Adam M. Oberman. How to train your neural ode: the world of jacobian and kinetic regularization. In *ICML*, pages 3154–3164, 2020.
- [48] Arash Vahdat, Karsten Kreis, and Jan Kautz. Score-based generative modeling in latent space. In A. Beygelzimer, Y. Dauphin, P. Liang, and J. Wortman Vaughan, editors, *Advances in Neural Information Processing Systems*, 2021.
- [49] Zhengzhong Tu, Jessie Lin, Yilin Wang, Balu Adsumilli, and Alan C. Bovik. Adaptive debanding filter. *IEEE Signal Processing Letters*, 27:1715–1719, 2020.
- [50] Jatin Sapra, Zhou Wang, and Akshay Kapoor. Capturing banding in images. 08 2021.
- [51] Michal Rolinek, Dominik Zietlow, and Georg Martius. Variational autoencoders pursue pca directions (by accident). In *Proceedings of the IEEE/CVF Conference on Computer Vision and Pattern Recognition*, pages 12406–12415, 2019.
- [52] Sunny Duan, Loic Matthey, Andre Saraiva, Nick Watters, Chris Burgess, Alexander Lerchner, and Irina Higgins. Unsupervised model selection for variational disentangled representation learning. In *International Conference on Learning Representations*, 2020.
- [53] Elliott Gordon-Rodríguez, Gabriel Loaiza-Ganem, and John P. Cunningham. The continuous categorical: a novel simplex-valued exponential family. In *ICML*, pages 3637–3647, 2020.
- [54] Aaron Van Den Oord, Oriol Vinyals, et al. Neural discrete representation learning. *Advances in neural information processing systems*, 30, 2017.
- [55] Rayhane Mama, Marc S. Tyndel, Hashiam Kadhim, Cole Clifford, and Ragavan Thurairatnam. NWT: towards natural audio-to-video generation with representation learning. *CoRR*, abs/2106.04283, 2021.
- [56] Alexei Baevski, Henry Zhou, Abdelrahman Mohamed, and Michael Auli. wav2vec 2.0: A framework for self-supervised learning of speech representations. *CoRR*, abs/2006.11477, 2020.
- [57] Kaiming He, Xiangyu Zhang, Shaoqing Ren, and Jian Sun. Deep residual learning for image recognition. In *2016 IEEE Conference on Computer Vision and Pattern Recognition (CVPR)*, pages 770–778, 2016.
- [58] James Bergstra and Yoshua Bengio. Random search for hyper-parameter optimization. *Journal of machine learning research*, 13(2), 2012.

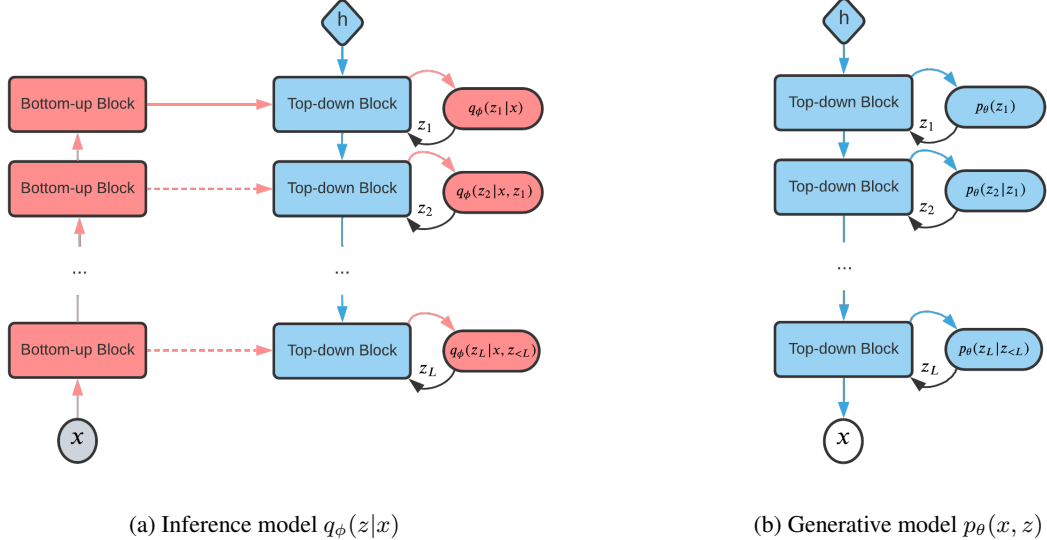


Figure 4: **Bidirectional inference HVAE.** The blue blocks are shared between the inference model and generative model. The inference model’s (encoder) outputs are in the bidirectional case computed by both a pass through the bottom-up then the top-down blocks. Dashed lines represent optional connections between the bottom-up and top-down blocks (more details in C.2 and the source code).

A Additional architecture details

A.1 General model architecture

We start by providing a more detailed information about the bidirectional HVAE architecture and how it works.

Figure 4 depicts the general form of a bidirectional inference HVAE, color-coded with: red for the inference model and blue for the generative model. Shared parameters between the inference and generative model are also coded in blue.

The bottom-up blocks in the HVAE extract latent activations χ that are used later on by the top-down block to create the posterior distribution $q_\phi(z_i|x, z_{<i})$. Both the prior and posterior distributions are created within the top-down block and are used in the KL divergence term of the ELBO.

During training, we sample z_i from the posterior $q_\phi(z_i|x, z_{<i})$ which depends on the activations χ computed by the bottom-up blocks. During unconditional generation from the prior, the bottom-up blocks are unavailable, we thus sample z_i from the prior $p_\theta(z_i|z_{<i})$ instead.

The VDVAE architecture is a special type of bidirectional HVAE, where the top-down block uses different bottleneck residual blocks[57] to compute the prior and posterior distributions. In figure 5c, we show the color-coded top-down block from VDVAE.

In Efficient-VDVAE, we make three slight modifications to the VDVAE architecture:

- **Bottom-up block:** We added a skip connection before propagating the output towards the top-down block. This enables us to project the activations χ to any arbitrary width when passing it to the posterior computation branch (in the top-down block), even if the filters number of the rest of the model is changing (figure 5b).
- **Pool layer:** VDVAE uses a non-trainable average pooling to downsample activations. We replace that with a 1×1 convolution to have the freedom to change the number of filters.
- **Unpool layer:** We add a 1×1 convolution prior to the nearest neighbor upsampling to also have the freedom to change the filter size inside the top-down model (figure 5a).

Although the VDVAE work raises the concern that using trainable convolutions in the "pool layer" and "unpool layer" can cause the low resolutions latent groups to not encode any information, we did not observe this behavior in our experiments. Nonetheless, should that happen on other datasets in the future, we provide the KL warm-up schedule described in NVAE[23] as a solution in the source code.

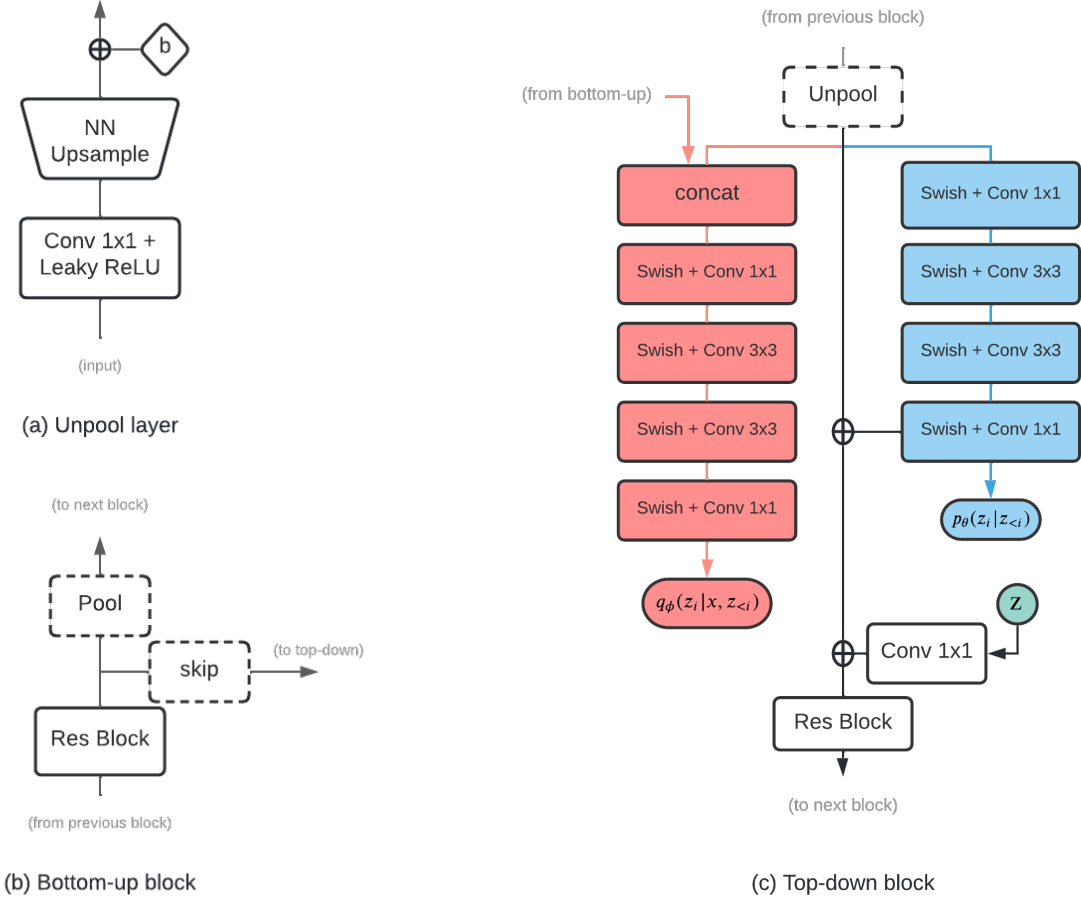


Figure 5: **Architecture of the Efficient-VDVAE.** Both the pooling and unpooling are different from the traditional VDVAE architecture for the sake of generalization of non-constant filter width in the model. The "Pool" layer is a convolution followed by a Leaky ReLU activation. Dashed blocks are optional and not always present (more details in the source code).

A.2 Detailed layer distributions parameters

In order to explain a part of the memory and NLL differences in table 3, we provide a more detailed overview of the distribution of the stochastic layers across different latent resolutions in table 6.

B Additional Results

B.1 Gradient smoothing and divergence

All the models in this work, including the CelebAHQ 1024×1024 and FFHQ 1024×1024 models, were trained with a maximal memory constraint of 320GB. As such, the maximum batch size that we were able to use on high resolution datasets is 8, which amplified the instabilities of not using gradient smoothing. As seen in table 2b, high resolution models cannot be trained without gradient smoothing as they very quickly diverge, despite our attempts of reducing the learning rate to account for the small batch size.

Dataset	Model	Latent resolutions	Layers per resolution
CIFAR-10	C1	$1^2, 4^2, 8^2, 16^2, 32^2$	3, 4, 7, 11, 22
	C2	$1^2, 4^2, 8^2, 16^2, 32^2$	3, 4, 7, 11, 22
	VDVAE	$1^2, 4^2, 8^2, 16^2, 32^2$	1, 3, 6, 11, 22
Imagenet 32 × 32	C1	$1^2, 4^2, 8^2, 16^2, 32^2$	6, 7, 19, 25, 16
	C2	$1^2, 4^2, 8^2, 16^2, 32^2$	6, 7, 19, 25, 16
	VDVAE	$1^2, 4^2, 8^2, 16^2, 32^2$	2, 5, 10, 20, 41
Imagenet 64 × 64	C1	$1^2, 4^2, 8^2, 16^2, 32^2, 64^2$	6, 7, 19, 25, 16, 11
	C2	$1^2, 4^2, 8^2, 16^2, 32^2, 64^2$	6, 7, 19, 25, 16, 11
	VDVAE	$1^2, 4^2, 8^2, 16^2, 32^2, 64^2$	2, 4, 8, 16, 32, 13
FFHQ 256 × 256	C1	$1^2, 4^2, 8^2, 16^2, 32^2, 64^2, 128^2, 256^2$	2, 4, 5, 10, 22, 14, 8, 1
	C2	$1^2, 4^2, 8^2, 16^2, 32^2, 64^2, 128^2, 256^2$	2, 4, 5, 10, 22, 14, 8, 1
	VDVAE	$1^2, 4^2, 8^2, 16^2, 32^2, 64^2, 128^2, 256^2$	2, 4, 5, 10, 22, 14, 8, 1

Table 6: Layers distribution by resolution.

Model depth	Without gradient smoothing		With gradient smoothing	
	NLL (bits/dim)	Skipped updates	NLL (bits/dim)	Skipped updates
30	2.28	2	2.27	0
49	2.20	9	2.21	1
66	2.18	14	2.18	0
69	2.18	24	2.17	0
75	2.17	37	2.17	2

Table 7: Effect of gradient smoothing with respect to model depth on 8-bit FFHQ 256 × 256 after 800k updates with $\beta = \log(2)$. The gradient smoothing doesn’t affect NLL, but greatly reduces the number of skips as the model gets deeper (All models were run with a batch size of 8).

B.2 Gradient smoothing and model depth

For completeness, we train networks while fixing all hyper-parameters and only changing the depth of the model. We then re-train the networks while removing the gradient smoothing and measure both NLL and the number of skipped updates. We show our results in table 7.

C Additional tips and insights for practitioners

In this section, we provide some notable tips and insights from our experience working with Efficient-VDVAE in the hope of saving valuable time for practitioners who want to use similar architectures.

C.1 Taming the exponentially growing variance of deep models

in their work[16], VDVAE’s author demonstrates how scaling the last convolution of each bottleneck residual block by $1/\sqrt{L}$, L being the total number of latent hierarchical variables, helps stabilize the model’s training. In their open sourced codebase, they additionally scale the weights of the projection of sample z (figure 5c).

When training under the Efficient-VDVAE setup, we observe that scaling the z projections is much more important than scaling the last convolution of each residual block. Not doing the former results in models diverging at the first training step, while not doing the latter can still result in models that train until convergence.

Network depth		Memory (GB)	NLL (bits/dim)
Bottom-up	Top-down		
22	47	13	2.90
27	47	15	2.89
33	47	17	2.87
40	47	20	2.87
47	47	22	2.87

Table 8: Effect of reducing the bottom-up model’s depth on CIFAR-10.

Distribution of Layers					Memory (GB)	NLL (bits/dim)
32×32	16×16	8×8	4×4	1×1		
0	11	7	4	3	9	2.96
11	11	7	4	3	13	2.91
22	11	7	4	3	17	2.87

Table 9: Effect of using high resolution layers on CIFAR-10. These results hold for all other datasets we tried except for MNIST because it has a binary distribution that we model using the Bernoulli distribution.

C.2 Asymmetrical model design

Traditionally, HVAEs were built to have symmetrical bottom-up and top-down models, where each top-down block i receives a different activation χ_i from a bottom-up block $L - i$. VDVAE breaks this symmetry by allowing K consecutive top-down blocks $\{i, i + 1, \dots, i + K\}$ to use the same activation χ_i . More specifically, χ_i is only extracted from the bottom-up model once per latent resolution, and is used for all top-down blocks of that resolution.

In our source code, we view these two designs as opposite extreme ends of the same general spectrum. In fact, we implement our models so that Efficient-VDVAE can be designed to be symmetrical, asymmetrical and any combination of the two (symmetrical in parts).

Empirically, for two models with the same number of layers, we didn’t notice any advantage to either design on NLL, convergence or stability. However, we experimented with reducing the bottom-up model’s size in an attempt to reduce computational requirements without hurting the model’s performance. We report our findings in table 8. We noticed that it is in fact possible to reduce the bottom-up model’s complexity up to a certain limit before starting to lose performance, as measured in NLL.

C.3 A note on the resolution of the latent space

We want to allocate this section to talk about the effect of building latent spaces in the same resolution of the input image.

While it is common practice in autoencoders to have a latent space smaller than the image so that the network compresses the pixel information and avoid learning an identity function, VAEs practically never learn an optimal latent space to model a distribution $p(x)$, even if they have the capacity to do so[18].

The implementation of latent spaces in the same resolution as the image can boost the NLL of the HVAE as shown in table 9. Qualitatively, however, these layers barely have a visible effect as they mostly operate on the noise of the pixels. Thus, if the goal is generative modeling, then the high resolution layers can be dropped for a memory load gain without major side effects.

C.4 A note on the overfitting of HVAEs

Like any other maximum likelihood model, HVAEs will overfit when they can. HVAE’s overfitting usually manifests as a large discrepancy between the aggregate posterior of the training data and the aggregate posterior of the validation data. This discrepancy can be measured by a difference between $D_{\text{KL}}(q_{\phi}(z|x) || p_{\theta}(z))$ in training and validation.

CIFAR-10 is a good example of when HVAEs (and maximum likelihood models in general) overfit, which is the main reason why models that rely on augmentations score better on that benchmark. CR-NVAE[44] is a good example

of an attempt to reduce the HVAE’s overfitting on CIFAR-10 by applying a consistency regularization on the latent space. While CR-NVAE was built on top of NVAE in their work, there should be no problem with applying the same consistency regularization to any other HVAE. That is however outside the scope of this work.

C.5 Keep a situational mindset

Despite the theory and the rules of thumb, it is always healthy to keep a situational mindset. At the end of the day, "For most data sets only a few of the hyper-parameters really matter, but [...] different hyper-parameters are important on different data sets"[58].

D Additional samples

D.1 Pruned posteriors reconstructions

We show in figure 6 reconstructions from Efficient-VDVAE before and after pruning 97% of its posteriors. Qualitative observations agree with the reconstruction loss, and no noticeable differences appear on the images. We hypothesize from these observations that the 3% of posteriors used in these reconstructions encode most of the latent information and they can be sufficient, and memory efficient, to use in downstream tasks.



Figure 6: Image reconstructions with 100% of the posteriors (left) and 3% of the posteriors with the highest average KL divergence (right). Both reconstructions are indistinguishable.

D.2 Generated samples from the prior

Due to lack of space in the paper, we share additional samples generated from the prior distribution here.



Figure 7: More unconditional samples on Imagenet 32×32 ($t = 0.85$).

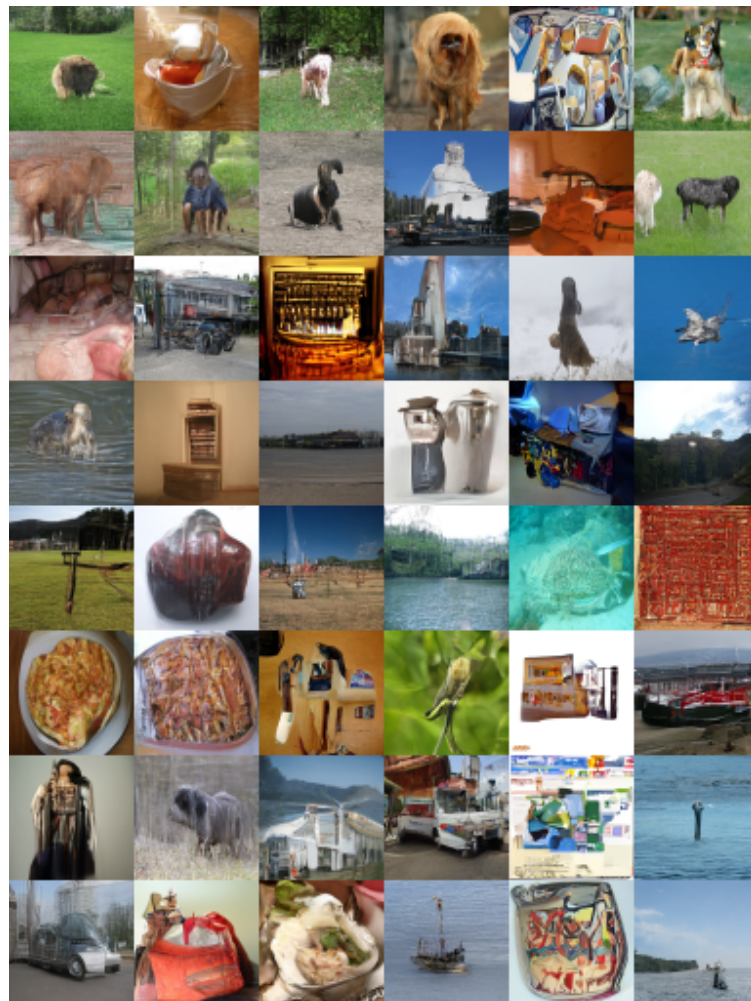


Figure 8: More unconditional samples on Imagenet 64×64 ($t = 0.9$).



Figure 9: Unconditional samples on MNIST ($t = 1$).



Figure 10: More unconditional samples on CelebA 64×64 ($t = 0.8$).



Figure 11: More unconditional samples on 5-bit CelebAHQ 256×256 ($t = 0.85$).



Figure 12: More unconditional samples on 8-bit CelebAHQ 256×256 ($t = 0.85$).



Figure 13: More unconditional samples on 5-bit FFHQ 256×256 ($t = 0.8$).



Figure 14: More unconditional samples on 8-bit FFHQ 256×256 ($t = 0.8$).



Figure 15: More unconditional samples on CelebAHQ 1024×1024 . From top row to bottom row, temperatures are $\{0.4, 0.6, 0.8, 1.\}$



Figure 16: More unconditional samples on FFHQ 1024×1024 . From top row to bottom row, temperatures are $\{0.3, 0.5, 0.7, 0.9\}$